Electronic Supplementary Information

for

Thermally-induced dimensionality change in a derivative of "super stable" Blatter radical

Bruno Camargo,[a] Irina Zajcewa,[b] Anna Pietrzak,[c] Emilia Obijalska,[d] Jacek Szczytko,[a] and Piotr Kaszyński* [d,e,f]

[a] Institute of Experimental Physics, Faculty of Physics, University of Warsaw, 02-093 Warsaw, Poland
[b] Institute of Physics, Polish Academy of Sciences, 02668 Warsaw, Poland.
[c] Faculty of Chemistry, Łódź University of Technology, 90-924 Łódź, Poland
[d] Faculty of Chemistry, University of Łódź, 91-403 Łódź, Poland
[e] Centre of Molecular and Macromolecular Studies, Polish Academy of Sciences, 90-363 Łódź, Poland
[f] Department of Chemistry, Middle Tennessee State University, Murfreesboro, TN, 37130, USA.

Table of Contents **Page**

1. Synthetic details

General. Commercially available solvents and reagents were used as received. The IR spectra were measured for neat compounds with an NEXUS FT-IR in KBr or Agilent Cary 630 FTIR spectrometers. Mass spectra were measured with a Varian 500-MS LC Ion Trap. High-resolution MS spectra were registered on Waters SYNAPT HDMS (ES+) or Waters SYNAPT G2-Si (AP+) mass spectrometers. Elemental analyses were obtained with a Vario EL III (Elementar Analysensysteme GmbH) instrument. Melting points were determined in capillaries with a Melt-Temp II apparatus and are uncorrected.

Preparation of radicals 1. General procedure. Bromoarene (0.70 mmol) was dissolved in anh. THF (1.0 mL) and a 1.9 M solution of *t*-BuLi in pentane (0.70 mL, 1.40 mmol) was added dropwise at –78 °C. After 15 min. the generated aryllithium solution was added dropwise at –78 °C to the solution of 3-phenyl-7-(trifluoromethyl)benzo[*e*][1,2,4]triazine[1] (**2**, 138 mg, 0.50 mmol) dissolved in anh. THF (2 mL). The reaction mixture was stirred for 1 hr at –78 °C, water (5 mL) was added (at –78 °C), opened to air and left stirring at ambient temperature for 1 hr. Reaction products were extracted with CH_2Cl_2 (4×) and the combined extracts were dried (Na_2SO_4). Solvents were removed and the resulting crude radical **1** was purified by filtration trough a SiO_2 pad using pet. ether with increased amounts of CH_2Cl_2 (0–70%) as the eluent.

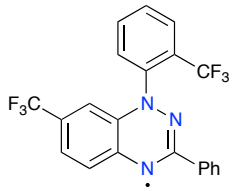

3-Phenyl-7-trifluoromethyl-1-(2-trifluoromethylphenyl)-1,4-dihydrobenzo[*e*][1,2,4]triazin-4-yl (1b). Yield: 200 mg (93%, Method B), dark brown crystals. Mp. 136–139°C (pet. ether/Et_2O), R_f = 0.81 (SiO_2, CH_2Cl_2/pet. ether 3:7). EPR (benzene) a_N = 7.51, 5.16 and 4.94, a_F = 3.65 G, g = 2.0034. IR (KBr) ν 3069w, 3034w, 1606w, 1496w, 1458m, 1426m, 1391s, 1353s, 1318s, 1264m, 1192m, 1128s, 1062m, 903m, 777m, 694m cm^{-1}. HRMS (TOF ES+) *m/z* $[M]^+$ calcd for $C_{21}H_{12}F_6N_3$: 420.0935, found 420.0935. Anal. Calcd. for $C_{21}H_{12}F_6N_3$ (420.09): C, 60.01: H, 2.88; N, 10.99. Found: C, 59.75; H, 3.00; N, 9.82.

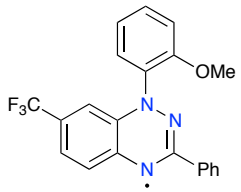

1-(2-Methoxyphenyl)-3-phenyl-7-trifluoromethyl-1,4-dihydrobenzo[*e*][1,2,4]triazin-4-yl (1c). Yield: 162 mg (95%, Method B); dark brown crystals. Mp 162–164°C (pet. ether/Et_2O), R_f = 0.60 (SiO_2, CH_2Cl_2/pet. ether 3:7). EPR (benzene) a_N = 7.50, 4.91 and 4.81, a_F = 3.36 G, g = 2.0034. IR (KBr) *v* 3075w, 3028w, 2977w, 2949w, 2844w, 1600m, 1499m, 1426m, 1397s, 1366s, 1321s, 1261s, 1063m, 1097s, 1065m, 1024m, 903m, 761m, 691m cm^{-1}. HRMS (TOF AP+) *m/z* $[M+1]^+$ calcd. for $C_{21}H_{16}F_3N_3O$: 383.1245, found 383.1241. Anal. Calcd. for $C_{21}H_{15}F_3N_3O$ (382.12): C, 65.97; H, 3.95; N 10.99. Found C, 66.00; H, 3.99; N, 10.74.

2. XRD data collection and refinement

Single-crystal XRD measurements for **1b** and **1c** were performed with a Rigaku XtalAB Synergy, Pilatus 300K diffractometer at 99.9(5) K using the CuK_α radiation (λ = 1.54184 Å). The data was integrated using CrysAlisPro program,[2] and intensities for absorption were corrected using multi-scan method as in SCALE3 ABSPACK scaling algorithm implemented in CrysAlisPro program.[2] Details are shown in Table S1.

Table S1. Selected structural data for 1b and 1c.

	1b CCDC: 2169663	**1c** CCDC: 2169662
Formula	$C_{21}H_{12}F_6N_3$	$C_{21}H_{15}F_3N_3O$
Formula Weight	420.34	382.36
Crystal System	triclinic	triclinic
Space Group	$P\bar{1}$	$P\bar{1}$
a /Å	7.9593(2)	4.5991(1)
b /Å	9.5462(2)	10.1298(3)
c /Å	13.0766(3)	19.1657(4)
α /°	87.499(3)	79.202(3)
β /°	78.856(2)	83.246(2)
γ /°	66.872(1)	77.704(1)
Volume /Å^3	895.92(4)	854.15(4)
Z	2	2
2θ range for data coll. /°	6.894 to 158.388	9.062 to 157.564
Index ranges	-9 ≤ h ≤ 10, -12 ≤ k ≤ 12, -16 ≤ l ≤ 16	-5 ≤ h ≤ 5, -12 ≤ k ≤ 10, -24 ≤ l ≤ 24
No. of measured, independent, and obs. [$I>2\sigma(I)$] reflections	20833, 3585, 3270	17481, 3531, 3165
*R*int	0.0285	0.0267
Goodness-of-fit on F^2	1.040	1.076
Final *R* indexes [$F^2>2\sigma(F^2)$]	R_1 =0.0326, wR_2 = 0.0880	R_1 =0.0365, wR_2 = 0.1028
Final *R* indexes [all data]	R_1 =0.0359 wR_2 = 0.0900	R_1 =0.0399 wR_2 = 0.1056
Data/restraints/ parameters	3585/0/271	3531/361/311
Largest diff. peak/hole /Å^{-3}	0.29/-0.29	0.25/-0.27

Structure solution and refinement

The structures were solved with the ShelXT[3] structure solution program using Intrinsic Phasing and refined in the ShelXle[4] by the full-matrix least-squares minimization on F^2 with the

ShelXL[5] refinement package. All non-hydrogen atoms were refined anisotropically and C–H hydrogens were generated geometrically using the HFIX command as in ShelXL. Hydrogen atoms were refined isotropically and constrained to ride on their parent atoms. In **1c** a disordered CF_3 group was identified. Sums of occupancies of relevant sites were set equal to 1 and refined using free variables. PART instruction was applied to exclude bonding between equivalent disordered atoms. Constraints and restraints such as EADP, SADI, DFIX, DANG, RIGU, and SIMU were used to aid disorders modeling. The CF_3 group in **1c** is disordered over three sites with the occupancy ratio 0.591(3):0.219(3):0.190(3).

The crystal data and structure refinement descriptors are presented in Table S1. Partial packing diagrams for **1b** and **1c** are shown in Figures S1–S4.

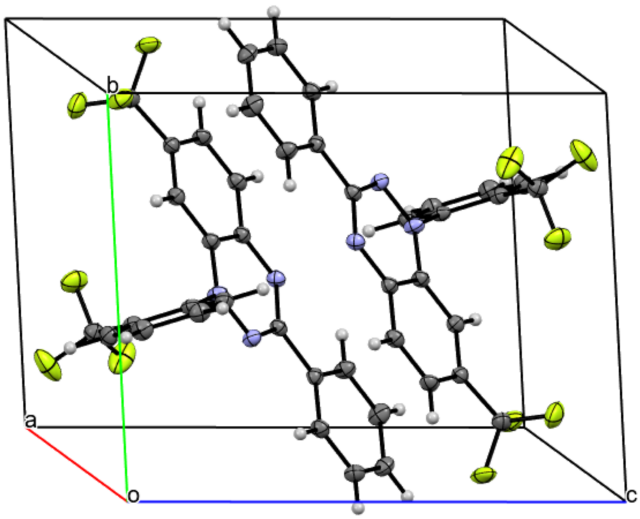

Figure S1. Unit cell packing diagram for **1b**. Color code: F-light green, N-blue

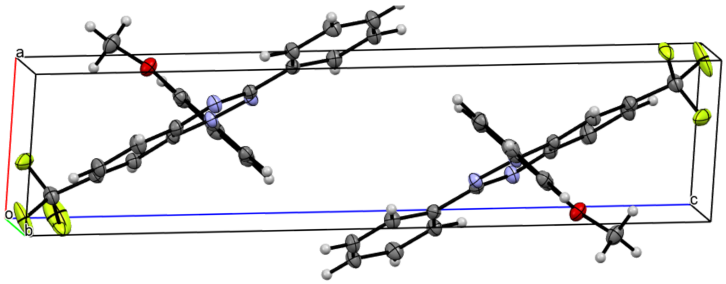

Figure S2. Unit cell packing diagram for **1c**. Color code: F-light green, N-blue, O-red

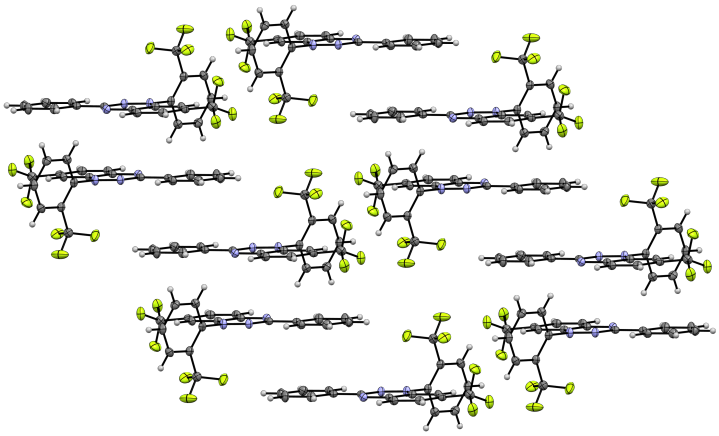

Figure S3. Slipped stacks of **1b**. Adjacent stacks are parallel to each other. Color code: F-light green, N-blue.

Close contacts within the stacks:

C(25)-H···F(1) 3.170 Å (-0.091 Å inside VDW separation)

C(15)-H···N(4) 2.713 Å (-0.037 Å inside VDW separation)

Close contacts between the stacks:

F(2)···F(5) 2.880 Å (-0.060 Å inside VDW separation)

Slippage angle - of 42.9° was calculated as an angle defined by C(3)···C(3)···C(8a) minus 90°. The two carbon atoms C(3) used for the measurements were for two molecules in the stack with same orientation.

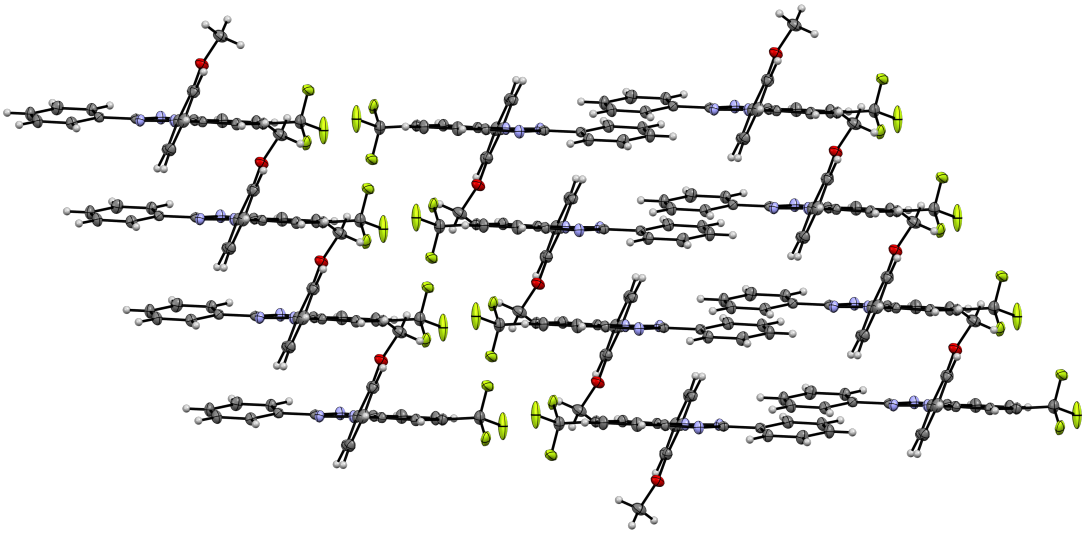

Figure S4. Slipped stacks of **1c**. Adjacent stacks are assembled parallel to each other. Color code: F-light green, N-blue, O-red.

Close contacts within the stacks:

C(8)-H···O 2.625 Å (-0.091 Å inside VDW separation)

C(Ar)-H···N(2) 2.683 Å (-0.067 Å inside VDW separation)

C(8)-H···O 2.625 Å (-0.095 Å inside VDW separation)

C(7)···F(1A) 3.115 Å (-0.055 Å inside VDW separation)

O-H···F(1A) 2.647 Å (-0.023 Å inside VDW separation)

C(Ar)-H···C(Ph) 2.689 Å (-0.031 Å inside VDW separation)

Close contacts between the stacks:

C(Ph)-H···C(Ar) 2.824 Å (-0.076 Å inside VDW separation)

C(7)-H···F(2A) 2.584 Å (-0.086 Å inside VDW separation)

F(2A)···F(2A) 2.756 Å (-0.184 Å inside VDW separation)

Slippage angle - of 36.6° was calculated as an angle defined by C(3)···C(3)···C(8a) minus 90°. The two carbon atoms C(3) used for the measurements were for two molecules in the stack with same orientation.

3. EPR spectroscopy

EPR spectra for radicals **1a**–**1c** were recorded on an X-band EMX-Nano EPR spectrometer at *ca*. 20 °C using dilute and degassed solutions in distilled benzene in a concentration range of 2–5×10^{-4} M. The microwave power was set with the Power Sweep program below the saturation of the signal, modulation frequency of 100 kHz, modulation amplitude of 0.5 G_{pp} and spectral width of 100 G. Accurate g-values were obtained using TEMPO as EMX-Nano internal standard. Simulations of the spectra were performed with *Easy Spin* (Matlab) including all nitrogen and fluorine atoms, and up to 10 different hydrogen atoms. The resulting *hfcc* values were perturbed several times until a global minimum for the fit was achieved. Experimental and simulated spectra are shown in Figures S5–S7 and resulting *hfcc* are listed in Table S2.

Figure S5. Experimental (blue, left), simulated (orange, right) and difference (grey, right) spectra for **1a** recorded in benzene at *ca* 20 °C.

Figure S6. Experimental (blue, left), simulated (orange, right) and difference (grey, right) spectra for **1b** recorded in benzene at *ca* 20 °C.

Figure S7. Experimental (blue, left), simulated (orange, right) and difference (grey, right) spectra for **1c** recorded in benzene at *ca* 20 °C.

Table S2. Experimental hyperfine coupling constants (G) and *g* values for radicals in series **1** recorded in benzene at 22 °C.

hfcc **/G**	**1a**	**1b**	**1c**
$a_{N(1)}$	7.58	7.51	7.50
$a_{N(2)}$	4.77	4.94	4.91
$a_{N(4)}$	4.87	5.16	4.81
$3\times a_F$	3.49	3.65	3.36
a_H	1.01	1.41	1.42
a_H	1.01	1.03	1.07
a_H	0.96	1.01	1.07
a_H	0.90	0.84	0.99
a_H	0.06	0.76	0.88
a_H	–	0.47	0.71
a_H	0.43(×2)	0.39	0.026
a_H	0.32(×2)	0.39	0.20
$2\times a_H$	0.18	0.62	0.88
$2\times a_H$	0.11	0.45	0.57
$3\times a_F$	–	0.42	–
g	2.0034	2.0034	2.0034

4. Magnetization measurements and data analysis

Magnetic susceptibility of polycrystalline samples was measured in a polycarbonate capsule fitted in a plastic straw as a function of temperature in heating (2 K→ 300 K) and cooling (300 K→ 2 K) modes with a sweep rate of 1 K min^{-1} at 0.25 T, using a SQUID magnetometer (Quantum Design MPMS-XL-7T). No significant differences in sample susceptibility were observed for data collected in both heating and cooling modes. Analysis was conducted for data obtained on cooling. Measurements of magnetization *M vs T* for **1c** were also conducted at several magnetic field strengths (0.05 –1 T) in a full temperature range.

Raw data workup

The capsule brings a large, constant diamagnetic component, which results in the magnetization curve crossing zero. Therefore, contribution of the capsule was removed by treatment of the data with a differential approach similar to that reported in ref.[6] Full details will be described elsewhere.

Molar magnetization curves for each compound were analyzed by fitting to a model described below.

1) Alternating antiferromagnetic chain of spins S = ½ based on the Hamiltonian (eq S1)

$$H = -2J \sum_{i=1}^{\frac{n}{2}} [S_{2i} S_{2i-1} + \alpha S_{2i} S_{2i+1}] \qquad \text{eq S1}$$

implemented in the Hatfield model[7] (the H model, eq S2):

$$\chi_H(T) = \frac{N_A g^2 \mu_B^2}{k_B T} \frac{A + Bx + Cx^2}{1 + Dx + Ex^2 + Fx^3} \qquad \text{eq S2}$$

$$x = |J|/k_B T$$

For $0 \leq \alpha \leq 0.4$:

$$A = 0.25$$

$$B = -0.062935 + 0.11376\alpha$$

$$C = 0.0047778 - 0.033268\alpha + 0.12742\alpha^2 - 0.32918\alpha^3 + 0.25203\alpha^4$$

$$D = 0.053860 + 0.70960\alpha$$

$$E = -0.00071302 - 0.10587\alpha + 0.54883\alpha^2 - 0.20603\alpha^3$$

$$F = 0.047193 - 0.0083778\alpha + 0.087256\alpha^2 - 2.7098\alpha^3 + 1.9798\alpha^4$$

where J- exchange integral (the first interaction parameter), α- the alternation parameter ≤ 1 (αJ- the second interaction parameter).

2) Paramagnetic susceptibility; the Brillouin model (the B model, eq S3):

$$\chi_B(T) = \frac{N_A g \mu_B}{B}\left(\frac{(S+0.5)}{\tanh\left((S+0.5) g\mu_B B/k_B T\right)} - \frac{0.5}{\tanh\left(0.5 g\mu_B B/k_B T\right)}\right) \qquad \text{(eq S3)}$$

For vanishingly low fields (B –> 0) it reduces to Curie law: $\chi_B(T) = \frac{N_A g^2 \mu_B^2 S(S+1)}{3k_B T}$

where N_A-Avogadro number, g-electron g-factor, μ_B-Bohr magneton,

k_B-Boltzmann constant, S-electron spin.

The above models were used to describe the experimental data for both radicals:

eq S4 for radical **1b**

$$\chi_{tot}T(T) = \chi_H T + \chi_d T \qquad \text{(eq S4)}$$

and eq S5 for radical **1c**:

$$\chi_{tot}T(T) = n_H \chi_H T + n_B \chi_B T + \chi_d T \qquad \text{(eq S5)}$$

where

χ_d- parameter of diamagnetic correction for the sample,

n_H *and* n_B - fractions of each model contributing to the total magnetic susceptibility.

i) Radical **1b**

A microcrystalline sample of derivative **1b** (m = 13.67 mg, 3.254×10^{-5} mol, M_w = 420.09 g mol^{-1}) at 0.25 T. Total molar magnetic susceptibility $\chi_{tot}(T)$ and $\chi_{tot}T(T)$ plots are shown in Figures S8 and S9, respectively. Fitting the latter data to the two-component model (eq 4) gave the diamagnetic susceptibility χ_d of –3.8(3)×10^{-4} cm^{3}mol^{-1}. The total magnetic susceptibility χ_{tot} was corrected for χ_d and the resulting paramagnetic susceptibility is plotted as $\chi_p T(T)$ in Figure S10.

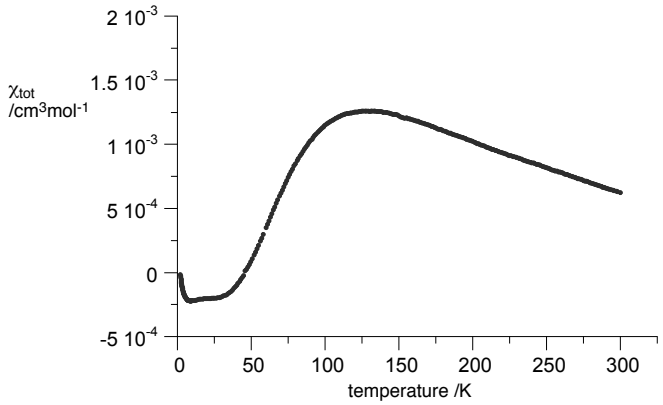

Figure S8. χ_{tot} *vs T* plot for **1b**.

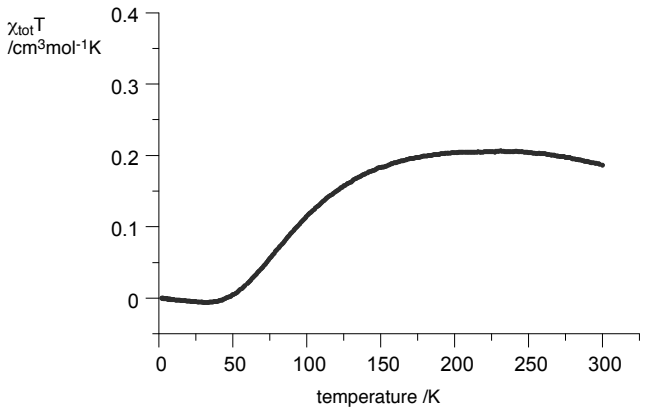

Figure S9. $\chi_{tot}T$ *vs T* plot for **1b**.

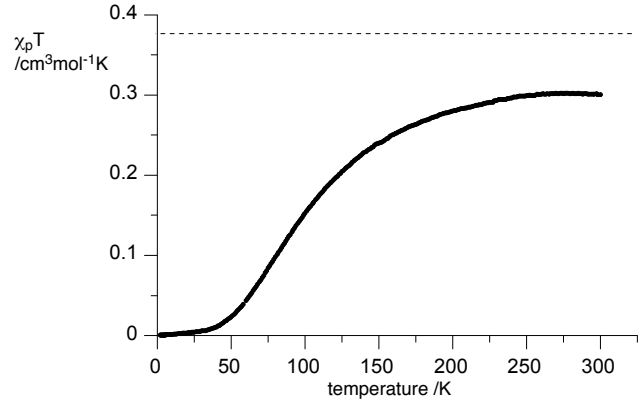

Figure S10. χ_pT *vs T* plot for **1b** after diamagnetic correction χ_d of -3.8×10^{-4} cm^3mol^{-1}. The horizontal line marks the Curie value of 0.375 Kcm^3mol^{-1} for an ideal paramagnet.

The diamagnetic correction obtained from the fitting compares to $\chi_d = -2.32\times10^{-4}$ cm^3mol^{-1} that can be calculated from Pascal constants.[8] The latter value is too small to bring the χ_pT curve to the range of all positive values.

ii) Radical **1c**

A microcrystalline sample of radical **1c** ($m = 22.42$ mg, 5.863×10^{-5} mol, $M_w = 382.4$ g mol^{-1}) was analyzed at 0.25 T. Total molar magnetic susceptibility $\chi_{tot}(T)$ and $\chi_{tot}T(T)$ plots are shown in Figures S11 and S12, respectively. Fitting the latter data to the three-component hybrid model (eq 5) gave the diamagnetic susceptibility χ_d of $-2.8(4)\times10^{-4}$ cm^3mol^{-1}. The total magnetic susceptibility χ_{tot} was corrected for χ_d and the resulting paramagnetic susceptibility is plotted as $\chi_pT(T)$ in Figure S13.

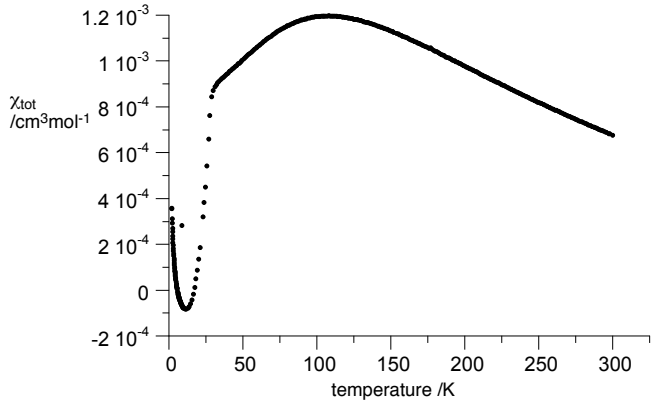

Figure S11. χ_{tot} *vs T* plot for **1c**.

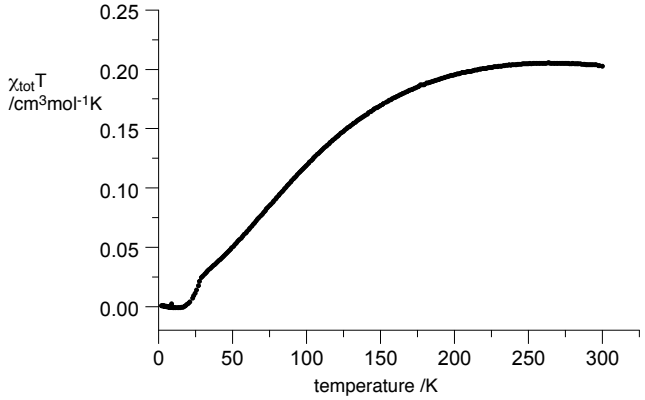

Figure S12. $\chi_{tot}T$ *vs T* plot for **1c**.

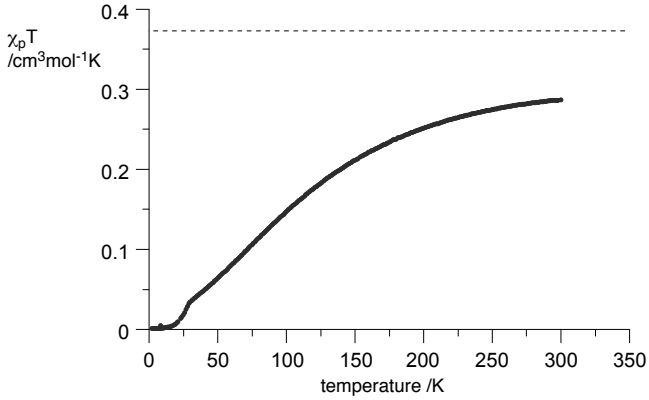

Figure S13. χ_pT *vs T* plot for **1c** after diamagnetic correction of -2.8×10^{-4} cm^3mol^{-1}. The horizontal line marks the Curie value of 0.375 Kcm^3mol^{-1} for an ideal paramagnet.

The diamagnetic correction value obtained from the fitting compares to $\chi_d = -2.27\times10^{-4}$ cm^3mol^{-1} calculated from Pascal constants.[8]

The total magnetic susceptibility of **1c** was measured at different field strengths up to 1 T, where the $M(H)$ remains approximately linear. The resulting χ_{tot} *vs T* plots show that the abrupt change in the magnetization curve takes place at the same temperature of 29 K (Figure S14).

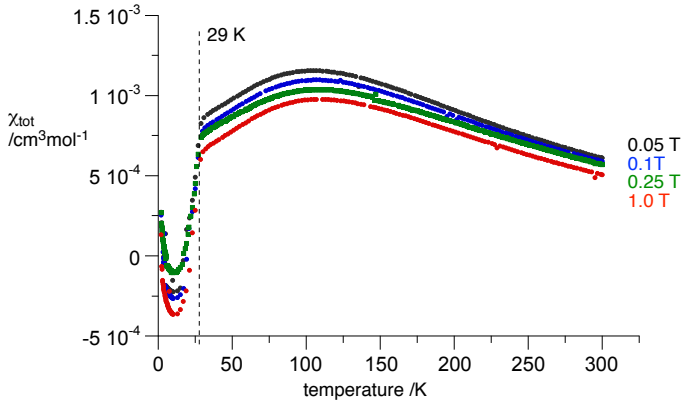

Figure S14. χ_{tot} *vs T* plots for **1c** at several field strengths 0.05–1.0 T.

5. References

1 A. Bodzioch, D. Pomikło, M. Celeda, A. Pietrzak, P. Kaszyński, *J. Org. Chem.,* 2019, **84**, 6377–6394.

2 Rigaku Oxford Diffraction (2020). CrysAlis CCD, CrysAlis RED, CrysAlisPro. Version 1.171.40.84a Rigaku Oxford Diffraction, Abingdon, England.

3 G. M. Sheldrick, *Acta Cryst., Sect. A,* 2015, **A71**, 3-8.

4 C. B. Hübschle, G. M. Sheldrick, B. Dittrich, *J. Appl. Cryst.,* 2011, **44**, 1281–1284.

5 G. M. Sheldrick, *Acta Cryst., Sect. C,* 2015, **C71**, 3-8.

6 R. Cabassi, F. Bolzoni, F. Casoli, *Meas. Sci. Technol.,* 2010, **21**, 035701.

7 J. W. Hall, W. E. Marsh, R. R. Weller, W. E. Hatfield, *Inorg. Chem.,* 1981, **20**, 1033–1037.

8 G. A. Bain, J. F. Berry, *J. Chem. Ed.,* 2008, **85**, 532–536.